Imaging spiral magnetic domains in Ho metal using circularly polarized Bragg diffraction

J. C. Lang, D. R. Lee, D. Haskel, and G. Srajer
Advanced Photon Source, Argonne National Laboratory, Argonne, Illinois 60439

(Presented on 6 January 2004)

We have used circularly polarized x rays to image the spiral magnetic domain structure in a single crystal of Ho metal. In these structures, the magnetization direction rotates between successive atomic layers forming a helix. At magnetic Bragg diffraction peaks, circularly polarized x rays are sensitive to the handedness of such a helix (i.e., either right or left handed). By reversing the helicity of the incident beam with phase-retarding optics and measuring the difference in the Bragg scattering, contrast between domains of opposing handedness can be obtained. © *2004 American Institute of Physics.* [DOI: 10.1063/1.1688252]

I. INTRODUCTION

In order to fully understand the magnetic properties of a material, the ability to measure its magnetic domain structure is essential. Many techniques have been developed to image magnetic domains, but most measure either ferromagnetic or linear antiferromagnetic structures.[1] A wide variety of materials, however, exhibit more exotic magnetic ordering, particularly materials containing rare earth elements. Spiral antiferromagnets are one such structure, where the moments align in ferromagnetic planes within an atomic layer but rotate by a characteristic angle between successive layers along the magnetic propagation direction. The sense of this rotation can be either right or left handed leading to the formation of chirality domains within the sample. In this paper, we describe a new technique for imaging this type of domain structure using circularly polarized x rays. Such domains have only been observed previously using neutron topography.[2] Using x rays to image spiral domains, however, can provide some unique advantages over neutron measurements, due to the element specific information obtained from x-ray measurements and the significantly higher achievable image resolution ($<1\ \mu$m).

The magnetic structure of Ho metal has been widely studied using both neutrons and x rays.[3–5] Ho orders magnetically in the spiral structure below $T_N=133$ K, with the propagation direction along the c axis of the hexagonal unit cell. Below $T=19$ K, the moments cant away from the basal plane forming a conical structure (Fig. 1). This magnetic super structure results in the appearance of satellite peaks on either side of charge Bragg diffraction peaks at $(0,0,L\pm\tau)$. The intensity of these magnetic peaks depends strongly on the energy of the incident x rays. Far from a resonance, the scattering cross section for a spiral magnetic structure is given by[6,7]

$$\frac{d\sigma}{d\Omega}=C\sin^2 2\theta\{S^2+2(L+S)^2\sin^2\theta+(2L\sin^2\theta+S)^2 - 4P_{\mathrm{lin}}[L\sin^2\theta(L\sin^2\theta+S)] \pm 4P_{\mathrm{circ}}\sin\theta(L+S)(L\sin^2\theta+S)\}. \quad (1)$$

Here C is a constant, L and S are the Fourier transforms of the spin and orbital magnetization, and P_{lin} and P_{circ} are the degrees of linear and circular polarization of the incident beam. The $\pm$ sign in the last term depends both on the magnetic wave vector (i.e., $\pm\tau$) and the handedness of the spiral (i.e., either right or left handed). Therefore, by using circularly polarized photons, the scattering becomes sensitive to the chirality of the magnetic structure. If the incident beam is small enough to scatter from a single chiral domain, the last term in Eq. (1) can be isolated by reversing the helicity of the beam ($\pm P_{\mathrm{circ}}$) and measuring the difference in the scattering intensity.

Magnetic x-ray scattering is an inherently weak process relative to charge scattering. Near an absorption edge, however, the magnetic scattering intensity can be strongly enhanced. The additional anomalous contributions to the scattering cross section from resonant terms can be calculated using the following expression:[8]

$$f_{EL}=4\pi\lambda\sum_{M=-L}^{L}(\epsilon_f^*\cdot\mathbf{Y}_{LM})(\mathbf{Y}_{LM}^*\cdot\epsilon_i)F_{LM}. \quad (2)$$

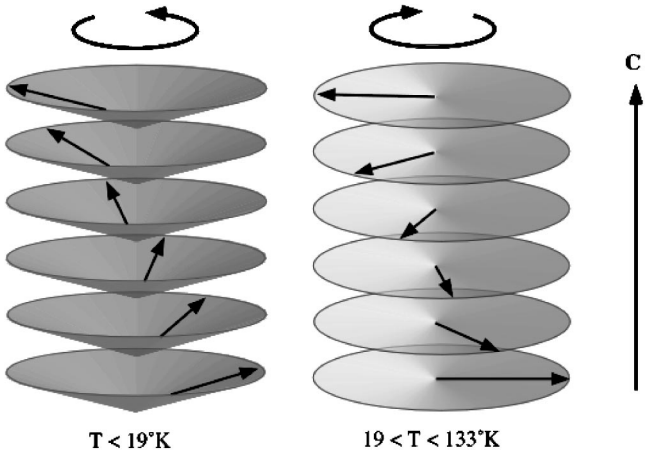

FIG. 1. The low temperature conical (left) and high temperature basal plane spiral (right) magnetic structure of Ho.

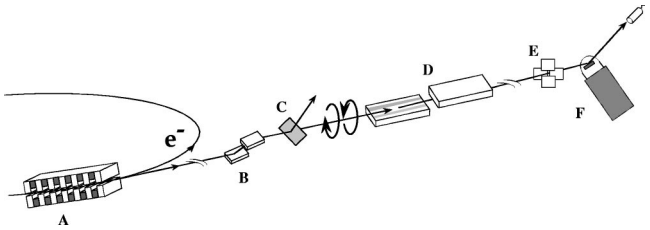

FIG. 2. Schematic of the experimental setup. The x-ray beam from the undulator (A) is monochromatized by a Si (111) double-crystal monochromator (B). The linearly polarized x-ray beam is then converted to a circularly polarized beam using a diamond (111) transmission phase retarder (C). A toroidal mirror (D) focuses the beam to $250\times100\ \mu m^2$ at the sample, and then slits (E) were used to further reduce the beam size to $25\times25\ \mu m^2$. The sample is placed inside a He refrigerator on a Huber goniometer (F).

Here ϵ is the beam polarization, Y_{LM} are vector spherical harmonics, and F_{LM} are the matrix elements of the transition. At resonance, the scattering still retains its sensitivity to the chirality of the magnetic structure, but its polarization dependent behavior is much more complicated than that given by Eq. (1) due to the presence of both dipolar and quadrupolar resonant terms.[9]

II. EXPERIMENT

The experiment was performed at the 4-ID-D insertion device beamline of the Advanced Photon Source.[10] A schematic of the experimental setup is shown in Figure 2. This beamline uses a standard planar undulator insertion device and a cryogenically cooled Si (111) double crystal monochromator. Synchrotron radiation is predominantly linearly polarized in the plane of the electron orbit. Therefore, a 400-μm-thick diamond (111) phase-retarder crystal in the Bragg transmission geometry was used to convert the incident linear polarization to circular.[11,12] The scattering plane of the phase retarder is inclined at 45° with respect to the synchrotron orbit plane. In this orientation, the phase retarder introduces a phase lag between the linear components of the transmitted beam. This phase lag is a function of the angular deviation from the Bragg diffraction condition, $\Delta\theta$, and can be adjusted to produce an x-ray beam with either positive or negative helicity ($P_{\mathrm{circ}}>0.98$). The helicity of the beam can be rapidly switched by rotating the phase retarder by a few tens of arcseconds. The beam was focused using a toroidal mirror to obtain a beam size of $250\times100\ \mu m^2$ at the sample position. This size beam yielded a photon flux on the sample of $\sim2\times10^{12}$ photons/s and was used for preliminary alignment of the sample. For the imaging measurements, however, the beam size was further reduced down to $25\times25\ \mu m^2$ using a set of slits immediately before the sample. It should be noted that, while the resolution for this measurement was $25\times25\ \mu m^2$, improved focusing optics can be used to obtain images with resolutions less than $1\ \mu m^2$.

The Ho crystal ($3\times3\times3\ mm^3$) used in this study was grown at Ames Laboratory. A c-axis face was oriented, mechanically polished, and finally electropolished yielding a sample mosaic width of $\sim0.02°$. The Ho crystal was placed inside a closed cycle He refrigerator ($T=7-350$ K), mounted on a Huber psi-circle goniometer. To obtain the chiral domain images, the sample was oriented on a magnetic Bragg peak and the goniometer and sample were scanned through the beam, reversing the helicity at each point.

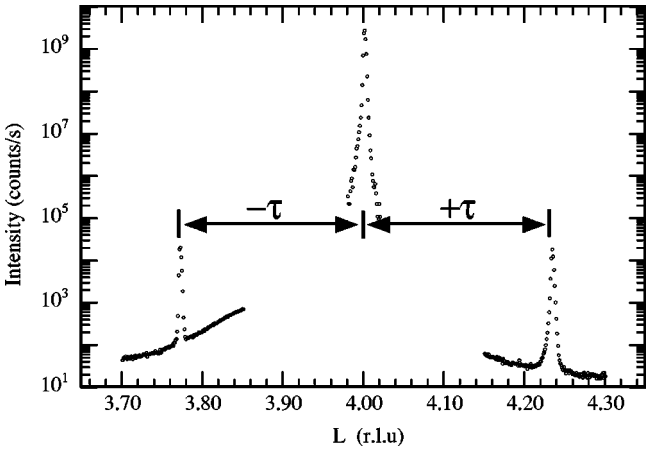

FIG. 3. X-ray scattering around the (0,0,4) Bragg reflection showing the $\pm\tau$ magnetic peaks at $T=60$ K.

III. RESULTS AND DISCUSSION

Figure 3 shows a scan through the (0,0,4) charge and the $\pm$ magnetic satellite peaks at $T=60$ K and $E=8.071$ keV. The intensity of the magnetic peaks is approximately five orders of magnitude smaller than the charge scattering peak at this temperature and energy. Near the L_3 edge absorption

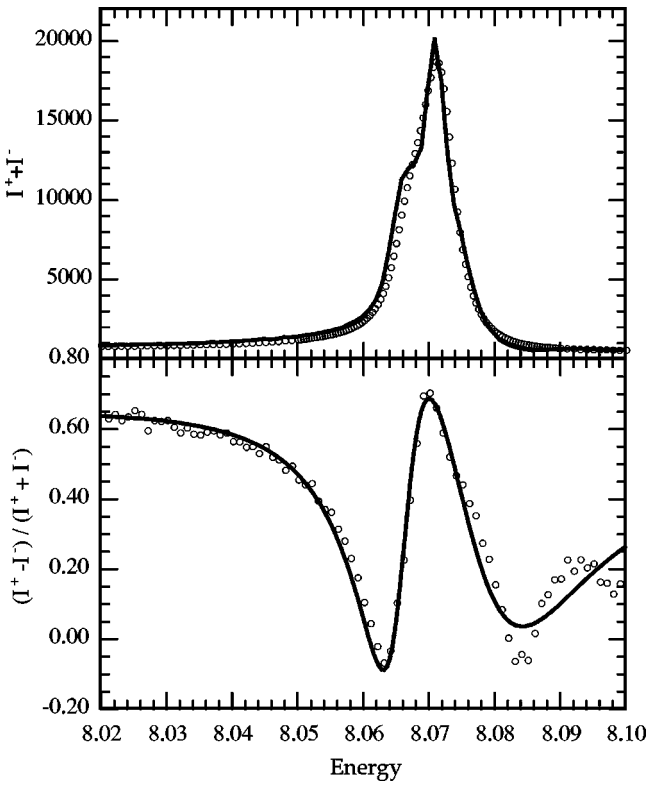

FIG. 4. Scattering intensity of magnetic peak with a circularly polarized incident beam. Top: Total counts. Bottom: Normalized difference. Line: Theory.

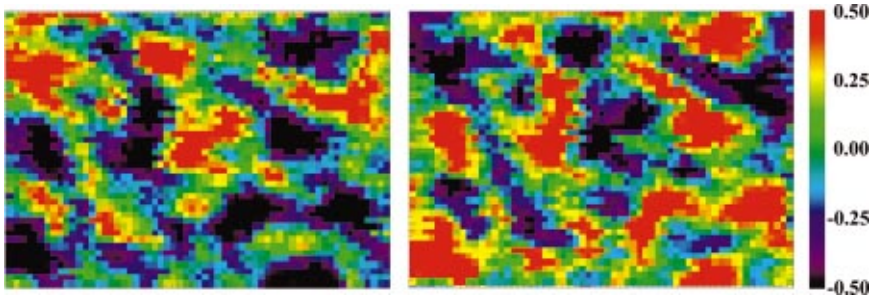

FIG. 5. (Color) Domain images ($600\times450\ \mu m^2$) taken at the $-\tau$(left) and $+\tau$(right) magnetic peaks.

resonance the scattering of the magnetic peaks is strongly enhanced due to the additional resonant terms. Figure 4 shows the energy dependence of the $(0,0,4+\tau)$ peak taken using a $25\times25\ \mu m^2$ circularly polarized beam. The top panel in Fig. 4 is a plot of the sum of the intensities taken with alternate helicities $(I^+ + I^-)$ showing the enhancement of the magnetic scattering, while the bottom panel is a plot of the normalized intensity difference, $(I^+ - I^-)/(I^+ + I^-)$. The lines in Fig. 4 are the expected behavior calculated using Eq. (2) and published matrix elements assuming scattering from a single chiral domain.[13] The strength of the contrast for experimental data matched the calculated curve well, suggesting that the small incident beam size isolated a single chiral domain. Similar scans taken with a $250\times250\ \mu m^2$ beam exhibited no helicity contrast. The maximum contrast of about 75% occurred about 1 eV below the peak of the scattering intensity, with contrast strongly suppressed on either side of the resonance. Away from the resonance, the contrast was similar to that at the peak, but, while it quickly approached this value below the edge, the contrast suppression persisted for over a hundred eV above the edge.

Images of the chiral domain structure were obtained by scanning the sample through the beam. Figure 5 shows two such $600\times450\ \mu m^2$ domain images taken at the $\pm\tau$ magnetic peaks. These images show a complete reversal of the contrast for each observed feature, as expected from Eq. (1). The features exhibit a characteristic length scale on the order of 50 μm consistent with previous neutron topography measurements.[2] The integral of each image was ~0.0 indicating that, over the length scale probed by these images, there were equal populations of each type of domain. Warming the sample past T_N and recooling nucleated a completely different domain pattern suggesting that crystalline defects play very little role in the nucleation of spiral domains. Furthermore, the features in these domains appear to be uncorrelated with the crystal lattice (a axis was oriented up in Figure 5).

In summary, we have successfully imaged the spiral domains in a Ho single crystal. The energy and wave vector dependence vary according to theoretical predictions. The observed structure of the spiral domains does not appear to correlate with the structure of the crystalline lattice.

ACKNOWLEDGMENTS

Work at Argonne is supported by the U.S. Department of Energy, Office of Science, under Contract No. W-31-109-ENG-38.

[1] R. J. Celotta, J. Unguris, M. H. Kelley, and D. T. Pierce, ''Techniques to measure magnetic domain structures,'' in *Methods in Materials Research: Current Protocols*, edited by E. Kaufmann (Wiley, New York, 2001), Chap. 6b.3.
[2] S. B. Palmer, J. Baruchel, A. Drillat, C. Patterson, and D. Fort, J. Magn. Magn. Mater. **54**, 1626 (1986).
[3] W. C. Koehler, J. W. Clable, M. K. Wlkinson, and E. O. Wollan, Phys. Rev. **151**, 414 (1966).
[4] G. P. Felcher, G. H. Lander, T. Arai, S. K. Sinha, and F. H. Spedding, Phys. Rev. B **13**, 3034 (1976).
[5] D. Gibbs, G. Grübel, D. R. Harshman, E. D. Isaacs, D. B. McWhan, D. Mills, and C. Vettier, Phys. Rev. Lett. **61**, 1241 (1988).
[6] M. Blume and D. Gibbs, Phys. Rev. B **37**, 1779 (1988).
[7] C. Sutter, G. Grübel, C. Vettier, F. de Bergevin, A. Stunault, D. Gibbs, and C. Giles, Phys. Rev. B **55**, 954 (1997).
[8] J. P. Hannon, G. T. Tramell, M. Blume, and D. Gibbs, Phys. Rev. Lett. **61**, 1245 (1988).
[9] J. P. Hill and D. F. McMorrow, Acta Crystallogr. **A52**, 236 (1996).
[10] J. W. Freeland, J. C. Lang, G. Srajer, R. W. Winarski, D. Shu, and D. M. Mills, Rev. Sci. Instrum. **73**, 1408 (2002).
[11] K. Hirano, T. Ishikawa, and S. Kikuta, Nucl. Instrum. Methods Phys. Res. A **A336**, 343 (1993).
[12] J. C. Lang and G. Srajer, Rev. Sci. Instrum. **66**, 1540 (1995).
[13] M. D. Hamrick Ph.D. Thesis, Rice University (1994).